Aerothermal Databases and Heat-Load Prediction for Re-Usable Launch Vehicle Configurations

Sebastian Karl[1], J. Wilken[2], L.Bussler[3]

Abstract

Orbital launch vehicles with re-useable major components or stages provide the potential to decrease the operational costs and to increase the flexibility of the entire system. DLR is conducting systematic studies of such configurations. The present analyses focus on different vertical take-off two stage systems which include a re-usable first stage. This stage is either configured for vertical landing using retro-propulsion or horizontal landing as a winged configuration. The layout and system analysis of such vehicles includes challenges related to the application of robust, light-weight, inexpensive and serviceable thermal protection systems. The thermal protection design requires accurate predictions of thermal loads for the entire atmospheric flight path. Due to the limitations and cost of ground based testing for large scale vehicles and the difficulty to apply general fluid mechanical scaling laws, these predictions rely intensively on numerical simulations (CFD). These CFD-based load predictions need to be coupled with an analysis of the structural response (heating model). Because of the large disparity of fluid mechanical and structural time scales, an unsteady CFD analysis over the entire trajectory is practically impossible and fast-response surrogate models for the aerothermal loads are required. This paper describes the structure and construction of such a model based on an aerothermal database. The database is composed of a series of steady-state CFD results which cover the entire atmospheric flight trajectory. Interpolation algorithms are used to estimate the local heating rate on each point of the vehicle surface as a function of flight time and local surface temperature. Particular challenges of the CFD analyses such as the plume-interactions during retro-propulsion maneuvers or the heat flux scaling depending on the local wall temperature are addressed. Exemplary applications and results of surface temperature predictions are shown.

Keywords: *aerothermodynamics, hypersonics, CFD, retro-propulsion*

---

[1] *DLR Institute of Aerodynamics and Flow Tech., Bunsenstr. 10, Göttingen (Germany), sebastian.karl@dlr.de*
[2] *DLR Institute of Space Systems, R.-Hooke-Str. 7, Bremen (Germany), jascha.wilken@dlr.de*
[3] *DLR Institute of Space Systems, R.-Hooke-Str. 7, Bremen (Germany), leonid.bussler@dlr.de*

Nomenclature

ATDB - Aerothermal Data Base
CFD – Computational Fluid Dynamics
GTO – Geostationary Transfer Orbit
HL – horizontal landing

LOx – liquid oxygen
RLV – Reusable Launch Vehicle
VL- vertical landing

1. Introduction

The recent success of SpaceX and Blue Origin in landing, recovering and relaunching complete launcher main stages has renewed the interest in the study of re-usable space transportation concepts (RLV). Previous systems with re-usable orbital segments, like the Space Shuttle, suffered from high system complexity and operational cost. Contrary to this, the limitation to the recovery of the first stage and the application of retro-propulsion for landing appears to be a promising concept for low-cost, robust and flexible launch vehicles.

DLR has initiated a systematic study on different concepts for re-usable first stages of large scale space launch systems within its XTRAS/ENTRAIN project [1, 2]. The primary goal of this study is to quantify the potential performance of retro-propulsion based vehicles in comparison to winged stages which perform horizontal landing. Further motivation arises from the lack of detailed data and information on the design and performance of recent operational RLV concepts in the open literature.

Generally, the design and basic layout of RLV configurations includes challenges related to the application of robust, light-weight, inexpensive and serviceable thermal protection systems (TPS). A major prerequisite for TPS sizing is the quantification of thermal loads. Therefore, one aspect of the present system studies is the generation of aerothermal data-bases (ATDB) for the accurate prediction of these loads over the entire flight trajectory. These ATDB consist of a set of CFD results for the surface heat fluxes at different trajectory points, operational conditions of the engines and surface temperatures. Together with appropriate interpolation algorithms, the ATDB constitutes a surrogate aerothermal model which enables quick estimates of the surface heat load at any flight time and surface temperature distribution.

While there is substantial experience in load predictions for hypersonic winged re-entry concepts, retro-propulsion maneuvers are a particularly challenging problem for both CFD and ground based testing. This is primarily due to the complex chemical and fluid mechanical interaction between the exhaust plume and the free stream. During retro-propulsion phases, large parts of the vehicle are immersed in its exhaust gases. Large recirculation regions and zones of flow reversal significantly affect the heat load distribution and aerodynamic characteristics. Because of the fuel-rich operation of rocket engines, additional heat release due to post-combustion is likely to occur which further influences the thermal budget of the flow.

This paper describes the CFD based generation and application of aerothermal databases for two exemplary first stage concepts for vertical and horizontal landing which are being developed in the DLR ENTRAIN study [1,2]. Both concepts belong to two-stage launch systems which are designed to deliver a payload of 7.5 tons to GTO.

2. General vehicle layout

The total length of the reusable main stages is about 40m and general schematics are shown in Fig.1. The vertically landing configuration (ENTRAIN-VL) uses LOx / methane as fuel in a cluster of 9 engines operating at a combustion pressure of 120bar and an oxidizer to fuel ratio of 3.3. For the horizontally landing winged configuration (ENTRAIN-HL) only the un-propelled re-entry flight is considered. The VL-configuration is shown in the left part of Fig. 1 with control surfaces in green, folded landing legs in blue, thrust nozzles in red and the fuselage in gray. The right part of this figure shows the HL-configuration with wings in green, fuselage in gray, control surfaces in blue and vertical stabilizers in light blue. Detailed information on system design, payload performance, flight trajectories and propulsion systems for both vehicles is given in [1] and [2].
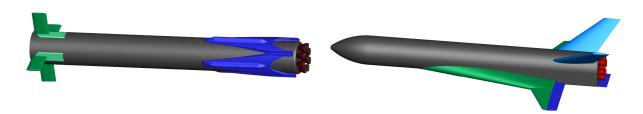
Fig 1. : Schematics of the first stage configurations for vertical (left) and horizontal (right) landing.

3. Numerical model

The heat flux distributions which are needed to populate the aerothermal data bases were obtained by CFD simulation of the flow field around both configurations. These numerical analyses were performed with hybrid structured–unstructured Navier–Stokes solver TAU [3]. The TAU code is a second-order finite-volume flow solver for the Euler and Navier–Stokes equations in their integral forms, using eddy viscosity, Reynolds stress or detached and large eddy simulation for turbulence modelling.

For the present investigation, we employed the Spalart–Allmaras one-equation eddy viscosity model [4]. The choice of the turbulence model was motivated by its ability to reproduce the structure of engine exhaust-plumes during retro-propulsion maneuvers [5] and by the general applicability for heat flux predictions in a wide range of hypersonic and reacting flow regimes [6-8]. The AUSMDV flux-vector splitting scheme was applied together with MUSCL gradient reconstruction to achieve second-order spatial accuracy whilst maintaining a robust numerical treatment of strong discontinuities.

The thermodynamic modelling is generally based on a mixture of thermally perfect gases. The properties of the individual species by are either computed from spectroscopic constants using partition functions that include an accurate representation of high temperature effects such as anharmonic-corrections and coupling of rotational and vibrational degrees of freedoms for molecules [9] or from NASA-Polynomials [10]. Appropriate mixture rules are applied to compute the thermodynamic properties depending on the local gas composition, pressure and density.

For the simulation of the EINTRAIN-VL vehicle, frozen and chemically reacting mixtures of air (76% N_2 and 24% O_2 by mass fraction) and engine exhaust gas (radially averaged composition at thrust nozzle exit of 16% CO, 38% CO_2, 44% H_2O and tracer species) are considered. The additional heat release due to post-combustion of the fuel-rich exhaust gases in the flow field around the rocket configuration is neglected for the ascent flight. During descent a global 3 step reaction mechanism [13] was employed to model this effect. This is justified by a set of preparatory investigations which are discussed in section 4.

The plume characteristic and exhaust gas composition at the thrust nozzle exit was obtained by a separate nozzle simulation. The flow was assumed to be in chemical non-equilibrium and a detailed $Ch4/O2$ reaction mechanism [11] was employed. The obtained flow profiles and the exhaust gas composition were then prescribed as an Dirichlet inlet conditions at the nozzle exit planes in the 3D simulations of the ENTRAIN rocket during the retro-maneuvers and the ascent flight.

The thermochemical modelling of the ENTRAIN-HL entry was based on an 11 species chemical equilibrium model for air. The maximum flight Mach number of 8.4 occurs at an altitude of 60km. Due to this moderate, sub-orbital flight speed and the large vehicle size, chemical non-equilibrium effects are not expected to significantly affect the surface heat flux distribution.

The computational domain includes a half domain for both vehicles. The hybrid / unstructured computational grids include approximately 7M grid points / volumes for the VL and 5M grid points for the HL configuration. All available geometrical details such as flap hinges and detailed geometry of the folded landing legs are retained in the discretized representation of the vehicles. Wall boundary layers are resolved with prismatic sublayers and a dimensionless wall spacing of y+ in the order of
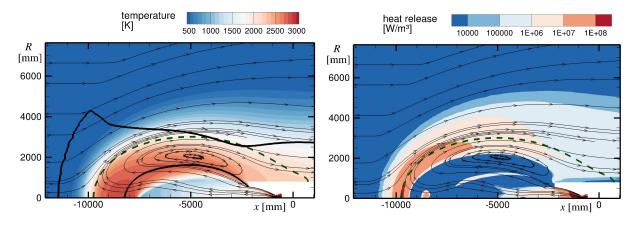
unity ensures appropriate resolution for the application of the low-Re formulation of the Spalart-Allmaras RANS turbulence model and for accurate heat flux estimations. The angle of attack was prescribed according to the trajectory analysis in a range from 7 to 0 deg for ENTRAIN-VL and from 40 to 5 deg for ENTRAIN HL.

4. Preparatory investigations
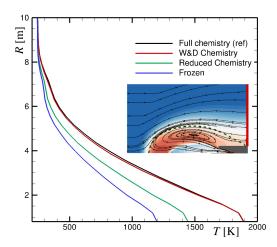
4.1. Air-exhaust chemistry

Due to the rich propellant mixture used in rocket engines, excess fuel is present in the exhaust plumes. This fuel can react with the ambient air. While it is expected, that chemical plume effects are of minor importance during ascent, the excess propellant in the exhaust jet is likely to ignite in the hot stagnation region of between the plume and the free stream during retro-propulsion maneuvers. The resulting exothermal post-combustion can significantly increase the flow temperature and, hence, the thermal surface loads. A simplified model problem was considered to identify an appropriate modeling strategy for post-combustion in LOX/methane plumes for the large scale simulations of the ENTRAIN-VL descent. This model problem consist of an axisymmetric representation of a single ENTRAIN-VL engine being operated at the design conditions of a combustor pressure of 120 bar and an oxidizer to fuel ratio of 3.3. The ambient free stream is at Mach 2 and a static pressure of 15 kPa. Post-combustion was treated with a detailed-chemistry approach based on a 20 species – 66 steps CH4 mechanism [11] ("full chemistry"), a skeletal 11 species – 7 steps mechanism [12] ("reduced chemistry") and a global Westbrook-Dryer 3 step mechanism [13] ("W&D chemistry"). The result for a chemically frozen exhaust jet is also added in Fig. 3 ("frozen").
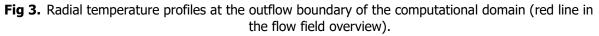
The resulting flow topology for the application of the detailed chemistry scheme is shown in Fig. 2. The sonic line is indicated in black and the line of flow reversal in green (dashed). The heat release distribution is depicted in the right part of the figure.
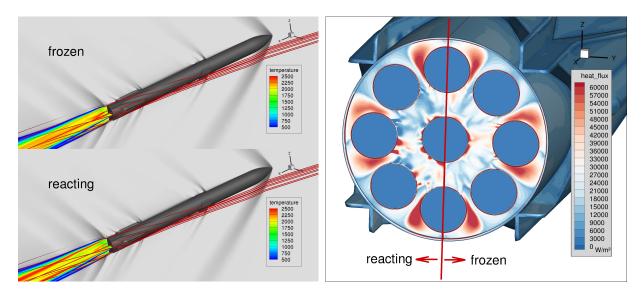

Fig 2. Model problem of a LOx/methane exhaust jet in a Mach 2 ambient flow, results from a detailed finite-rate model [10], left: Temperature distribution, right heat release

A comparison of radial temperature profiles resulting from the application of different reaction mechanisms is given in Fig. 3. The effect of post combustion significantly increases the gas temperature in the vicinity of the launcher surface. The difference between the frozen calculation (neglect of post-combustion) and the results for full chemistry and the global Westbrook-Dryer mechanism is about 700K close to the surface ($R = 1$ m in Fig. 3). The global mechanism is able to accurately reproduce the reference temperature profile of the detailed mechanism. Hence it was selected for the compelx 3D simulations.

Fig 3. Radial temperature profiles at the outflow boundary of the computational domain (red line in the flow field overview).

The influence of the chemical heat release in the plume on the numerical results for the ascent flight of ENTRAIN-VL was assessed based on a preliminary design iteration of the first launcher stage. This initial design was discontinued due to the occurrence of excessive base heating and system challenges to realize engine gimbaling. The global 3-step combustion mechanism was applied for these analyses. The flight Mach number is 1.5 and the atmospheric pressure is 25kPa. The results in are shown in Fig. 4 and demonstrate that the influence on the base heating is negligible although the temperature distribution in the exhaust plume is significantly affected by post-combustion.
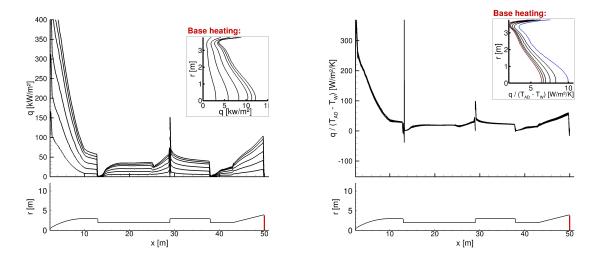

Fig 4. Comparison of plume temperatures and base heating patterns for frozen and reacting ascent simulations (grey colours: qualitative Mach number distribution in the symmetry plane)

4.2. Thermal wall boundary conditions

A model for the dependency of the local wall heat transfer on the surface temperature is required in an aerothermal database. The concept of heat transfer coefficients allows an efficient and accurate estimate of this relation on the basis of local adiabatic wall temperatures. However, this concept may be prone to errors in zones with large flow separation which occur in the present study during retro-maneuvers and in the base region. Hence, a dedicated preparatory study was performed to asses the accuracy of wall heat flux estimations based on a distribution of heat transfer coefficients. An axi-

symmetric generic rocket configurations was analyzed which contains relevant features such as forward/backward facing steps, a flare and a blunt base. The free stream conditions correspond to a flight Mach number of 7. Heat flux distributions for a range of wall temperatures between 200K and 1800K and the adiabatic wall temperature distribution were obtained by separate CFD analyses.

The heat flux distributions for the ascent flight are shown in Fig. 5. The exhaust plume was omitted in the corresponding simulations. The heat flux distribution on the base (marked in red in the schematic) is shown in separate plots. The right part of Fig. 5 depicts the distribution of the heat transfer coefficient (heat flux scaled by the difference of local wall temperature and adiabatic wall temperature). All results for wall temperatures between 200 and 1800 K collapse to a single line. Exceptions are distortions in the vicinity of the forward and backward facing steps, and, most importantly, the base region. The local disturbances near surface steps and cavities are due to different size of flow separation zones at different wall temperatures. Here, the heat transfer coefficient strongly depends on the wall temperature and can not be applied for a simplified estimate of the dependency of the heat flux on the wall temperature.

Fig 5. Heat flux distribution on a generic rocket configuration at Mach 7 for a range of wall temperatures between 200 and 1800 K. Left: absolute heat flux, right: heat transfer coefficient.

Surface heat flux distributions at different wall temperatures between 200 and 1800 K during a retro-propulsion maneuver at Mach 7 are shown in Fig. 6. A schematic of the resulting flow field is depicted in the upper right part of the sub-figures. As compared to the results in Fig. 5, the general level of surface heat flux is significantly reduced by the presence of the retro-plume at the present hypersonic flight conditions.

The right part of Fig. 6 shows the heat transfer coefficients for the retro-propulsion case. A residual scatter of about 17% is observed. This is significantly less than for the separated base flow in the ascent case (Fig. 5). Again, due to the temperature dependence of the heat transfer coefficient for those flow topologies, it can not be applied for a simplified estimate of wall heat fluxes.

Due to the observed applicability limits of heat transfer coefficients for flows with large scale recirculation zones, the prediction of surface temperature dependency of the wall heat flux in the ENTRAIN data bases was based on a linear interpolation between CFD solutions at different isothermal wall temperatures.
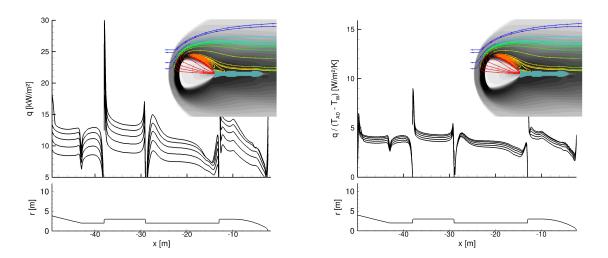
Fig 6. Heat flux distribution on a generic rocket configuration at Mach 7 during a retro-propulsion maneuver for a range of wall temperatures between 200 and 1800 K. Left: absolute heat flux, right: heat transfer coefficient.

4.3. Summary of the applied modelling strategy

The preparatory investigations have led to the following applied modeling strategies:

- ENTRAIN-VL, ascent: frozen exhaust chemistry, CFD simulations for wall temperatures of 200, 400, 600 and 800 K

- ENTRAIN-VL, descent: reacting exhaust gas (3-step global mechanism), CFD simulations for wall temperatures of 200, 500 and 800 K

- EINTRAIN-HL: chemical equilibrium model for high temperature air, CFD simulations for wall temperatures of 200, 500, 800 and 1100 K

5. Database generation end exemplary CFD results

For the ENTRAIN-VL launcher, 8 trajectory points for the ascent phase and 11 for the re-entry and descent phase were considered for detailed CFD analyses. A set of 11 CFD simulations was carried out to obtain detailed surface heat flux distributions for the population of the ENTRAIN-HL data base. These sampling points are summarized in Fig. 7. The flight trajectory with engine-off conditions is shown as a black line. The red line in Fig. 7 (b) denotes engine operation during retro-burn and landing maneuvers. The labeled circles depict the trajectory points for which CFD flow field analyses were performed. Each sub figure contains the velocity-altitude curve (labelled with "v") and the time-altitude curve, labelled with "t"). Each of these CFD investigations was performed for a range of different wall temperatures as detailed in section 4.3. The angle of attack was varied according to the trajectory and flight analysis [1,2] from 40deg to 5 deg for ENTRAIN-HL and from 10 to 1 deg for ENTRAIN-VL.

For the Entrain-VL configuration, the heat loads during ascent are generally lower as during descent. Significant base heating occurs only during high-altitude flight where the associated large spreading of the exhaust plumes results in a strong recirculation of hot exhaust gases towards the rocket structure. This phenomenon is illustrated in Fig. 8. The colors in the symmetry planes represent exhaust gas mass fraction and the gray iso-surfaces depict zones of flow reversal. The left and part of the figure represent low and high altitude operation, respectively. The gray iso-surfaces in this figure show the development of strong stagnation and flow reversal zones between the thrust nozzles during high altitude operations. This effect develops rapidly at flight altitudes above 20km.

For the ascent flight, it was found that the wall temperature has a distinct influence on the aerodynamic drag causing variations of up to 7% at flight Mach numbers of around 5. The reason is that the boundary layer thickness and the size of shock induced separation bubbles change which alters the surface pressure at windward protrusions (mainly upstream surfaces of the landing legs)
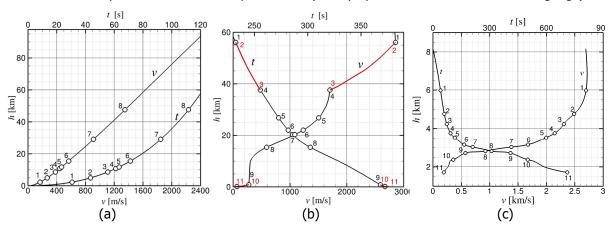

Fig 7. CFD population of the aerothermal databases. (a): ENTRAIN-VL, ascent, (b): ENTRAIN-VL, descent, (c): ENTRAIN-HL, descent
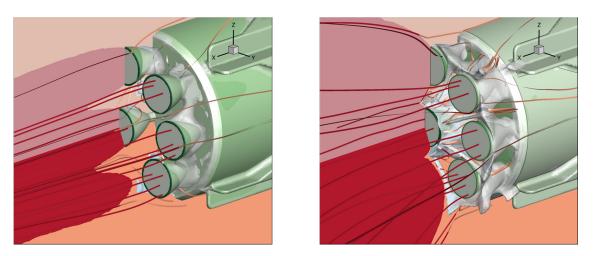

Fig 8. Different base flow patterns during ascent

During descent, global peak heating occurs during the un-propelled high-speed flight after the retro-maneuver. While the exhaust plume during retro-burns efficiently shields the base region of the rocket from excessive thermal loads, it generates high heat fluxes at the protrusions and control surface leading edges.

A typical flow field during un-propelled flight of the ENTRAIN-VL configuration is shown in Fig. 9 for a flight Mach number of 8.9. The distribution of surface heat flux is shown in color and the static pressure across the symmetry plane is shown in gray-scale. The bow shock is close to the base plate and the flow passes through the cluster of thrust nozzles. Strong axial vortices are generated in this region. These vortical structures are convected downstream and result in a complex pattern of surface heating on the base plate an on the upstream part of the landing legs. Strong local heat peaks are observed at shock impingement locations (e.g. visible on the upper fin in Fig. 9). Due to the continuously changing flight conditions, the location of this impingement points are not stationary and no adverse impact on the integrated heat load was observed.

A typical flow field result which corresponds to the initiation of the first retro-burn at an altitude of 56 km and a flight Mach number of 8.9 is shown in Fig. 10 (left). The brown iso-surface indicates the extent of the exhaust gases which completely immerse the vehicle. Again, the surface heat flux distribution is shown in color scale, the gray scale across the symmetry plane represents flow temperature. Peak flow temperatures occur in the stagnation region between the exhaust jet and the incoming free stream. This hot gas is then immersing the entire vehicle. Due to the moderate densities and the flow essentially being aligned parallel to the vehicle surface, the heat fluxes remain moderate. The highest thermal loads during retro-burn occur at the control surfaces which directly face the incoming exhaust flow being heated in the upstream stagnation zone.

The flow topology in the base of the launcher changes at low altitude conditions to a similar pattern as for ascent. A representative flow field solution is shown in Fig. 10(right) for a flight Mach number of 0.2 at an altitude of 200m. Due to the large ambient pressure, the exhaust jets are constricted and due to the low flight Mach number and associated low free stream momentum the flow reversal of the exhaust gases is significantly reduced. The heat loads during this flight regime are generally not critical (below 20kW/m² for a wall temperature of 200K)
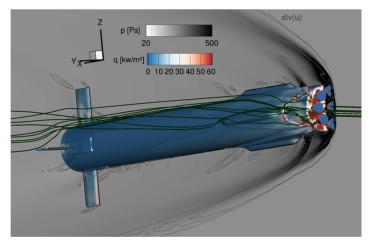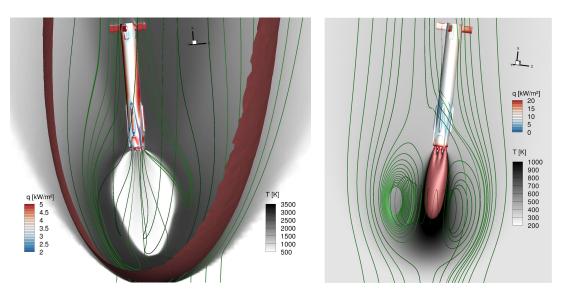

Fig 9. Flow field during hypersonic descent before initiation of first retro-burn

Fig 10. VL-configuration: Exemplary flow field at the beginning of the retro-maneuver (left) and during the subsonic landing burn (right)

A representative solution for peak heating conditions of the ENTRAIN HL-configuration (trajectory point #4 in Fig. 7(c)) is shown in Fig. 11. Surface heat flux is shown in color and Mach number in gray scale The right part of the figure shows a representative heat flux profile on the outboard wing section. At the corresponding flight Mach number of 6.8, the wing span is larger than the radius of the bow shock of the main fuselage. This results in a strong shock-interaction being visible at the outboard wing section in Fig. 11. The local heat flux is increased by approximately a factor of 3.5. However, this local amplification is exists only during a small portion of the flight time (at Mach numbers below 5.5, the entire vehicle is immersed in the bow shock and no strong interactions occur) and, during its existence, it constantly moves in outboard direction. Hence, the effect on the overall heat load at the wings remains comparatively small. Critical loads occur at the leading edges of the outboard wing section due to their comparatively small radius. Further, fuselage nose cone and the deflected control surfaces suffer from high heat fluxes. The vertical stabilizers operate in the wake of the vehicle and are therefore protected from excessive heat loads.
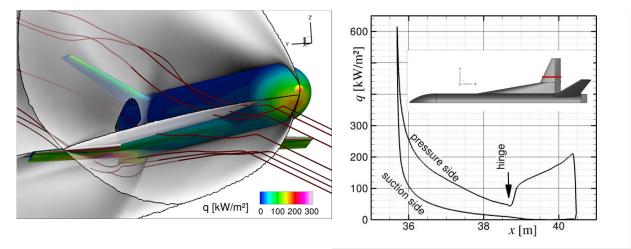

Fig 11. HL configuration, representative flow field at peak heating conditions

The detailed local heat flux data from the CFD analyses are stored in aerothermal databases. Together with appropriate interpolation algorithms, these databases constitute fast response models to estimate the local heat flux at each point of the surface as a function of the current flight time and the local wall temperature. The data bases for the aerothermodynamic heating can be easily coupled to a structural response model to evaluate the temperature history during atmospheric flight for each location on the vehicle surface as shown in section 6.

6. Exemplary applications of the aerothermal databases

As outlined in the section 5, the purpose of the Aerothermal Database (ATDB) is to provide data for the estimation of the surface heat transfer on the vehicle especially during the flight regimes which impose strong thermal loads (hypersonic flight, retro-propulsion maneuvers). It serves as a surrogate model for the aerothermal heating which is valid for any flight time during heating phases and for any distribution of surface temperatures. The ATDB consists of a structured set of CFD results and includes the surface heat flux distributions at different temperatures and trajectory points.

To illustrate the coupling process and the application of the aerothermal database, the local surface temperature histories of both the ENTRAIN-VL ascent and descent configurations and of the ENTRAIN-HL configuration are computed during the entire atmospheric flight path.

A simple lumped mass model that represents instantaneous heating of a 5mm aluminium structure was employed for this example. The material properties are summarized in the following table:

Surface emissivity	$\varepsilon =$	0.2	[-]
Wall thickness	$\delta =$	5	mm
Density	$\rho =$	2600	kg/m³
Heat capacity	$c =$	900	J/kg/K

Table 1. Material properties of the lumped mass model

The coupling algorithm consists of the following steps:

(1)	Assume an initial constant surface temperature of T_0=200K at the beginning of the entry flight at a trajectory time. Set current time $t = t_0$ Set current surface temperature $T(x, y, z) = T_0$
(2)	Interpolate the convective heat flux distribution, $q_c(x, y, z)$ for the current flight time, t, and the current surface temperature distribution $T(x, y, z)$ using the interpolation functions of the aerothermal database
(3)	Compute the local surface radiation as the difference of radiative surface emission and incoming background radiation: $$q_r = \varepsilon\sigma T_W^4(x,y,z) - \sigma T_\infty^4$$
(4)	Update the distribution of local wall temperatures after a time step of Δt: $$T_{new}(x,y,z) = T(x,y,z) + \Delta t\,(q_c(x,y,z) - q_r(x,y,z))\,/\,\delta\rho c$$
(5)	Set $T(x, y, z) = T_{new}(x, y, z)$ and repeat from step (2) until the desired final flight time is reached

The simple structural response model in step (4) can be easily replaced by a more elaborate analysis for more detailed investigations. The basic engineering model here serves as an exemplary application.

ENTRAIN-VL results of the exemplary database application as outlined in the algorithm above are shown in Fig. 12(left) for the ascent flight and Fig. 17 (right) for descent. The most critical component for both, the ascent and descent, configurations is the base plate. Significant heat loads occur at the windward surfaces of protrusions (e.g. landing legs) and the leading edges of the control surfaces. The main cylindrical body of the rocket does not experience critical heat loads.
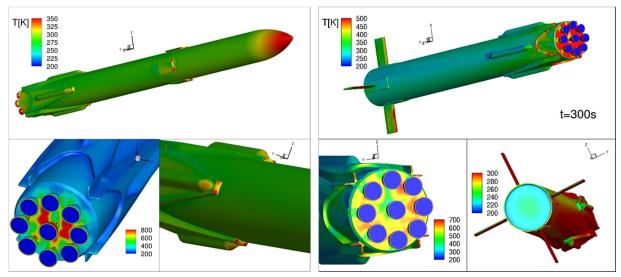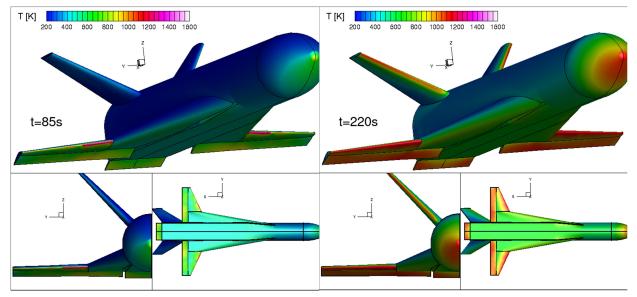

Fig 12. Surface temperature distribution at the end of the ascent flight (left), Peak surface temperatures during descent (right).

Representative results for structural heating for the ENTRAIN-HL configuration are summarized in Fig. 13. The left part shows the temperatures at hypersonic flight during peak heating conditions. Strong local heating due to the interaction of the vehicle bow shock and the outboard wings is clearly visible in the vicinity of the outboard wing leading edge. The right part of the figure shows the peak surface temperature distribution which occurs at a flight time of about 220s. After this time, the cooling effect of the surface radiation exceeds convective heating and the surface temperatures decrease. The most critical components which require dedicated TPS are the nose cone, the outboard wings, the leading edges of the vertical stabilizers and the control surfaces.

Fig 13. Surface temperature distributions from the lumped mass model, left: peak heating conditions, right: maximum surface temperatures reached during re-entry flight.

Heat load histories during the atmospheric descent are shown in Fig. 14 for both configurations. For ENTRAIN-VL, the base plate is the most critical component. The protective effect of the exhaust jets during the retro-propulsion maneuver is clearly visible between a flight time of 230 and 255s. After 295 s, the heat flux on the base plate becomes negative, the radiative cooling exceeds the convective heating. The control surfaces (green line) are subjected to significant heat loads during the operation of the engines between 230 and 255s and after 370s. This is due to the impact of hot exhaust gases.
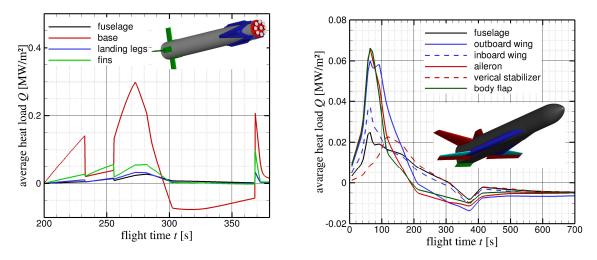

Fig 14. Heat load histories during the atmospheric descent of ENTRAIN-VL (left) and ENTRAIN-HL (right)

The peak heating of the ENTRAIN-HL configuration occurs around a flight time of 80s (right part of Fig. 14). The peak loads on the vertical control surfaces occur after a delay of about 30s. This is due to the variation of the angle of attack from 40deg to 10deg which results in an increasing exposure of the vertical stabilizers to the free stream (initially at large AoA located in the wake of the fuselage). The most critical components are the outboard wings and the control surfaces. Although the average heat loads are lower than for the HL-configurations, the local peak values at the leading edges are significantly larger.

6.1. Density-velocity scaling of integrated heat loads

The integrated heat load on the entire ENTRAIN-VL vehicle is shown in Fig. 15 for two assumed constant wall temperatures of 200K and 500K. The figure further includes the flight velocity and free stream density (red and green dashed line, respectively). The circles represent the detailed CFD results for all flight conditions without retro-propulsion. The solid lines correspond to a heat flux variation according to a scaling of the form $q = k\rho^A u^B (1-h/h_W)$. The linear constant k is used to match the total heat load levels and is identical for both curves. The term h/h_W is the ratio of total to wall enthalpy. The exponents A and B are calibrated to values of 0.92 and 2.8, respectively. They differ from their classic values of $A=0.5$ and $B=3$ (e.g. Sutton-Graves, Chapman correlations). This difference is attributed to the present complex flow structure (base plate in the wake of the thrust nozzles, large flat-plate-like regions). Nevertheless, the present modified scaling law can potentially be applied to increase the interpolation accuracy in future database applications.
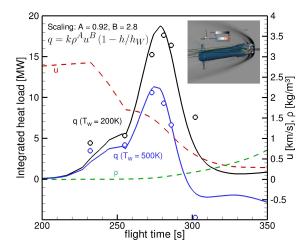

Fig 15. Density-velocity scaling for the ENTRAIN-VL descent flight

7. Conclusion

A set of CFD investigations for the ENTRAIN-VL and EINTRAIN-HL configurations was carried out for different flight conditions (trajectory points) and wall temperatures. The resulting detailed local surface heat flux distributions were assembled in three aerothermal databases for the different vehicle concepts. These databases also include interpolation algorithms which provide local surface heat flux estimates for all flight times and wall temperature distributions and, as such, form fast-response surrogate models for the aerothermal heating. The function of the databases was demonstrated by the computation of the complete local wall temperature histories for the entire atmospheric flight of both vehicles based on a basic lumped-mass structural model. It was found that the retro-jets of the ENTRAIN-HL configurations efficiently protect the base region from excessive heat loads while exposing the control surfaces to additional heating. The most critical components are the base plate (VL-configuration) and the wing leading edges and control surfaces (HL-configuration).

Auxiliary studies showed that the concept of heat transfer coefficient is not applicable to the present complex flow fields and multiple CFD solutions at different wall temperatures are required for a

correct representation of the dependency of heat flux on local wall temperature. Further, the modelling of the chemical heat release caused by the post-combustion of excessive fuel in the exhaust jet is necessary for the accurate representation of the gas properties in the vicinity of the VL-vehicle during descent.

An attempt to reproduce the heat load history along the flight trajectory with a density-velocity scaling law showed promising results but, due to the complex flow fields, further investigation and adaptation to specific cases appears to be required.

References

1. Stappert, S., Wilken, J., Sippel, M., Dietlein, I.: Evaluation of European Reusable VTVL Booster Stages, IAA Space and Astronautics Forum and Exposition, 17-19 September 2018, Orlando, Florida, USA

2. Wilken, J. et al: Multidisciplinary Design Analysis of Reusable European VTHL and VTVL Booster Stages, Proceedings HiSST 2020, 2020

3. Langer, S., Schwöppe, A., and Kroll, N.,"The DLR Flow Solver TAU—Status and Recent Algorithmic Developments," AIAA Paper 2014-0080, 2014

4. Spalart, P.R., and Allmaras, S.R.,"A One-Equation Turbulence Model for Aerodynamic Flows," AIAA Paper 1992-0439, 1992.

5. Ecker, T., Karl, S., Dumont, E., Stappert, S. Krause, D., "Numerical Study on the Thermal Loads During a Supersonic Rocket Retropropulsion Maneuver," Journal of Spacecraft and Rockets, electronic pre-print ,https://doi.org/10.2514/1.A34486, 2019

6. Fechter, Stefan und Karl, Sebastian und Hannemann, Volker und Hannemann, Klaus (2017) Simulation of LOx/GH2 single coaxial injector at high pressure conditions. AIAA/SAE/ASEE Joint Propulsion Conference, AIAA Propulsion and Energy Forum, 10.-12. Juli 2017, Atlanta, GA, USA. DOI: 10.2514/6.2017-4765

7. Klaus Hannemann · Sebastian Karl Jan Martinez Schramm · Johan Steelant, Methodology of a combined ground based testing and numerical modelling analysis of supersonic combustion flow paths, Shock Waves (2010) 20:353–366, DOI 10.1007/s00193-010-0269-8

8. Karl, S. "Numerical Investigation of a generic Scramjet Engine," PhD-Thesis, TU-Dresden, 2011, available online: https://nbn-resolving.org/urn:nbn:de:bsz:14-qucosa-68695

9. Bottin B.: Aerothermodynamic Model of an Inductively-Coupled Plasma Wind Tunnel. PhD-Thesis University of Liege, 1999

10. Gordon S., McBride B. J.: Computer Program for Calculation of Complex Chemical Equilibrium Compositions and Applications. NASA Reference Publication 1311, 1994

11. Slavinskaya, N.A., Haidn, O.J., Steelant, J.: Kinetic Modeling for High Pressure, Fuel - Rich Methane / Oxygen Combustion, AIAA Paper 2007-0775, 45th AIAA Aerospace Sciences Meeting and Exhibit, Reno, Nevada, 2007

12. Schneider, D., Genin, C., Stark, R., Oschwald M.: Numerical Model for Nozzle Flow Application Under Liquid Oxygen/Methane Hot-Flow Conditions, J. Propulsion and Power 34(1), 2018

13. Wang, L., Liu, Z., Chen, S. Zheng Z.,: Comparison of Different Global Combustion Mechanisms Under Hot and Diluted Oxidation Conditions, Combustion Science and Technology, 184:2, 259-276 (2012)